IEICE TRANS. INF. & SYST., VOL.E93–D, NO.2 FEBRUARY 2010

PAPER

A Novel Modeling and Evaluating for RTS Noise on CMOS Image Sensor in Motion Picture

Deng ZHANG[†a)], **Jegoon RYU**[†], ***Student Members, and*** **Toshihiro NISHIMURA**[†], ***Member***

SUMMARY The precise noise modeling of complementary metal oxide semiconductor image sensor (CMOS image sensor: CIS) is a significant key in understanding the noise source mechanisms, optimizing sensor design, designing noise reduction circuit, and enhancing image quality. Therefore, this paper presents an accurate random telegraph signal (RTS) noise analysis model and a novel quantitative evaluation method in motion picture for the visual sensory evaluation of CIS. In this paper, two main works will be introduced. One is that the exposure process of a video camera is simulated, in which a Gaussian noise and an RTS noise in pinned-photodiode CMOS pixels are modeled in time domain and spatial domain; the other is that a new video quality evaluation method for RTS noise is proposed. Simulation results obtained reveal that the proposed noise modeling for CIS can approximate its physical process and the proposed video quality evaluation method for RTS noise performs effectively as compared to other evaluation methods. Based on the experimental results, conclusions on how the spatial distribution of an RTS noise affects the quality of motion picture are carried out.

key words: *CMOS image sensor, noise modeling, random telegraph signal noise, video quality*

1. Introduction

With the increasing demand for human vision, how to export higher quality images and video becomes the central consideration for the design of next generation of image sensor. The higher quality image refers to an image with higher resolution and having less noise. At present there exists typically two classes of image sensor in the market, complementary metal oxide semiconductor image sensor (CMOS image sensor: CIS) and Charge Coupled Device (CCD). On one hand, the drawback of CIS is its higher noise than CCD. On the other hand, its strength is fewer components, lower power consumption and faster data acquisition. More important is that the subminiature pixel to achieve high resolution by means of CIS is easier to be implemented due to the highly developed technology for CMOS devices production [1], [2].

However, problems also appear at the time of downscaling of CIS pixel. One of them is low-frequency (LF) noise, which leads to a significantly perceptual impact on motion pictures and consists of a Gaussian component noise and a non-Gaussian component noise referring to a Random Telegraph Signal (RTS) noise [3]. And the RTS noise is a

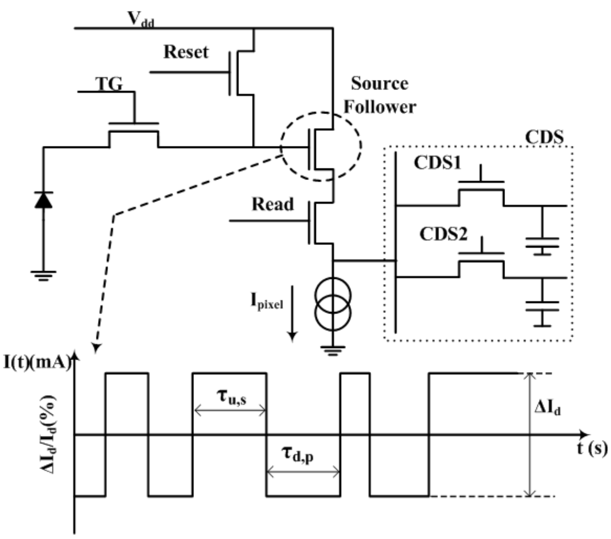

Fig. 1 A two-level RTS noise example.

fluctuation in current or voltage with random discrete impulses of equal heights resulting from carrier trapping and de-trapping into single oxide defect in the surface of Source Follower transistor [4]. For example, a two-level RTS noise is shown in Fig. 1, where $\tau_{u,s}$ and $\tau_{d,p}$ are the s-th and p-th duration of an impulse in the up and down time respectively, and ΔI is the amplitude of the RTS noise.

Cost control for canceling RTS noise source comes up as another problem caused by the downscaling of CIS pixel. The reason is that the single oxide defect cancelation in the surface of MOSFETs is extremely difficult and has high cost for CIS manufacturing process. And the cost is almost proportionate to the number of pixels having to be de-defected.

According to the two problems mentioned above, we have to decrease the cost as much as possible on the premise of which the distortion of motion pictures could be ignored. As a consequence, we need an accurate noise model of CIS in order to estimate the degree of distortion in a motion picture degraded by LF noise, especially RTS noise.

In the previous works based on Shockley-Read-Hall model [5], the theoretical foundation of RTS noise, a probability density function (PDF) or a noise power spectral density (P.S.D) function of the observed signal used to be calculated in time domain [6]–[8] or in frequency domain [4], [9]–[11]. Besides, Konczakowska [3], [12] proposes a novel approach to identify RTS noise of semiconductor devices. However, all these research concentrate on the behavior or

Manuscript received May 14, 2009.
Manuscript revised September 14, 2009.

[†]The authors are with the Graduate School of Information, Production, and Systems, Waseda University, Kitakyushu-shi, 808–0135 Japan.
a) E-mail: zhdnstar@fuji.waseda.jp

DOI: 10.1587/transinf.E93.D.350

characteristics of RTS noise in a single CIS pixel in time domain, in frequency domain or both of them based on experiments on physical devices. On the contrary, Kobayashi [13], Wang [14] describe the spatial distribution of RTS noise but still merely give physical experimental results. Nevertheless researchers are always in need of the mathematical modeling of RTS noise to analyze and reduce RTS noise in motion pictures, which is a more convenient but less costly tool to study the mechanism of RTS noise and its impact on motion pictures compared with the physical methods. From this point of view, Picinbono [15] analyzes the RTS using statistical method, but it is also limited to the individual RTS behavior.

Based on the accurate modeling of the RTS noise of CIS, we then need a proper tool to evaluate the video quality degraded by RTS noise. Peak signal-to-noise ratio (PSNR) is the most easily calculated and widely adopted image and video quality evaluation method. However, PSNR is somewhat a mean value in nature. Recently a number of video quality metrics which motivate human visual sensitivity based on spacial contrast sensitivity function have been proposed, i.e., just noticeable distortion [16]–[18]. There are also some video quality evaluation methods focusing on compressed motion pictures using discrete cosine transform (DCT), i.e., Movie Quality Evaluation (MQE) [19], Video Quality Matrix (VQM) [20] and Digital Video Quality (DVQ) [21]. Ji [22] even applies fuzzy synthetic judgment to evaluate the compressed video. However, almost all of the related works on video quality mentioned above either calculate some mean values or require a huge computing complexity, which is ineffective for RTS noise case by the reason that only several percent of pixels on a CIS have single oxide defect in the surface of Source Follower.

Calculating those parameters in time domain or in frequency domain is definitely helpful to estimate the mechanism of RTS noise in a single CIS pixel. However, an image usually consists of millions of pixel instead of a single pixel. Thus, it is more significant to study and evaluate the collective behavior of RTS noise on an image sensor than that in a single CIS pixel. In order to solve the two problems introduced above, we propose a precise noise modeling of CIS in motion pictures and develop an effective video quality evaluation method in this paper.

This paper is organized as follows. Section 2 firstly presents a motion picture simulator with newly proposed RTS noise model, which is concerned primarily with the spatial distribution of its noise source on a CIS instead of a single pixel. Section 3 shows the proposed video quality evaluation method for RTS noise on a CIS in motion pictures which is named as RTS Video Quality (RTS_VQ). Using this simulator with RTS_VQ, the sensory rating of CIS imaging with RTS noise is obtained by our video quality evaluation method. And experimental results are summarized in Sect. 4. Eventually, the conclusion is presented in Sect. 5.

2. Proposed RTS Noise Model

The proposed RTS noise model in this study consists of a Gaussian component noise and a non-Gaussian component noise [3]. To intuitively observe the perceptual impact on motion pictures of the proposed noise modeling, we add it onto a motion picture whose frames are all Macbeth chart as shown in Fig. 2 [23]–[26] by means of simulating the exposure process of a digital camera. The flowchart of the exposure process of a digital video camera is given as Fig. 3, and the proposed modeling is one of its physical processes.

For digital camera, the output of a pixel on a CIS is a three dimensional quantity, $P_{i,j}(k)$, $i \in [1, M]$, $j \in [1, N]$, $k \in [1, K]$, where i and j are the location of pixel in spatial domain and k is its calibration in time domain; M, N are the size of the CIS, and K is the number of frames as shown in Fig. 4. To evaluate the fluctuation of the proposed noise modeling in the time domain, quantity noise level denoted as NL is proposed and defined as (1)–(3),

$$P_{i,j}(k) = f(v_{i,j}(k)) \tag{1}$$

$$\sigma_{i,j}^2 = \frac{1}{K} \times \sum_{k=1}^{K} P_{i,j}^2(k) - \overline{P_{i,j}(k)}^2 \tag{2}$$

$$NL_{i,j} = \frac{1}{g_c} \times \sigma_{i,j} \tag{3}$$

where $v_{i,j}(k)$, $\sigma_{i,j}^2$, and $NL_{i,j}$ are the output, variance and noise level of pixel $P_{i,j}$, and g_c is the noise gain of analog-to-digital conversion. Based on the definition of NL, another quantity, noise histogram, which is the histogram of NL of all pixels of CIS, has been proposed to describe the spatial distribution of RTS noise sources with different noise levels on a CIS.

2.1 Gaussian Component Noise Modeling

According to the shape of noise histogram, dark current shot noise and dark current FPN, thermal noise, reset noise, 1/f noise, and light FPN are modeled as the Gaussian component noise. Table 1 shows the detail information about all these noise mentioned above, where k is the Boltzmann constant, T is Kelvin temperature, g_m is the gain of the conductance between transistors, C is capacitance, e is the charge

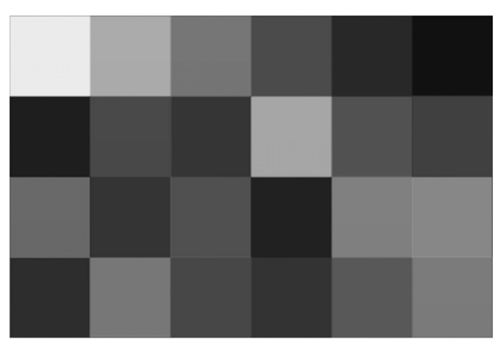

Fig. 2 Noise free Macbeth chart.

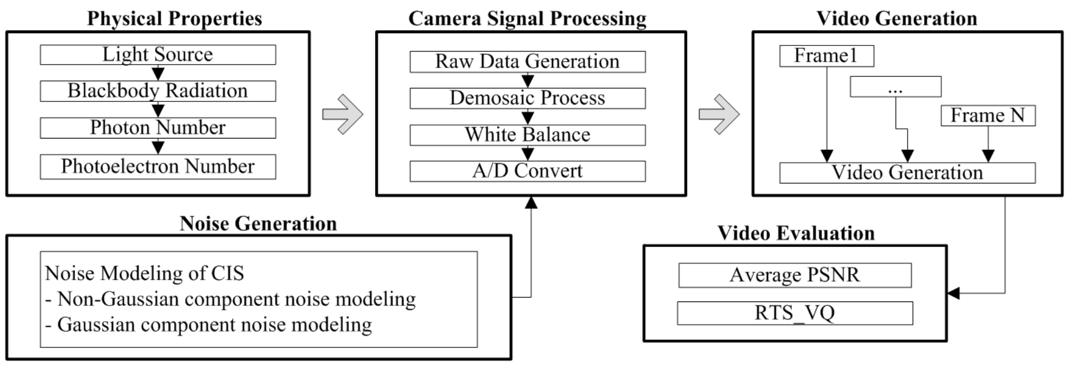

Fig. 3 Flowchart of the exposure process of a digital video camera.

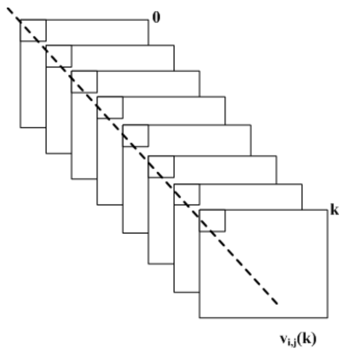

Fig. 4 Pixel output of pixel (i, j) in frame sequence.

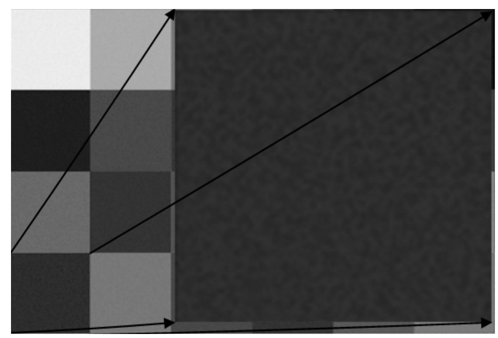

Fig. 5 Noisy Macbeth chart with the Gaussian component noise.

Table 1 Gaussian component noise list.

Noise Type	Distribution	μ	σ
dark current shot noise	Poisson	-	-
dark current FPN	Weibull	-	-
thermal noise	Gaussian	0	$\sqrt{4kT/g_m}$
reset noise	Gaussian	0	$\sqrt{kTC}/e$
1/f noise	Gaussian	0	$\sigma_{1/f}$
light FPN	Gaussian	0	σ_{lFPN}

of one electron, and σ_{lFPN} and $\sigma_{1/f}$ are the standard deviation of light FPN and 1/f noise respectively. The value of σ_{lFPN} is related to the photon number and $\sigma_{1/f}$ is defined as (4)–(8),

$$\sigma_{1/f1} = \frac{1}{\eta_{pin}} \int_{1}^{10^6} \frac{K_{flicker} I_p}{\sqrt{La_p Wa_p f}} df \tag{4}$$

$$\sigma_{1/f2} = \frac{1}{\eta_{pin}} \int_{1}^{10^6} \frac{K_{flicker} I_c}{\sqrt{La_c Wa_c f}} df \tag{5}$$

$$\sigma_{1/f3} = \frac{1}{\eta_{pin}} \int_{1}^{10^6} \frac{K_{flicker} I_p}{\sqrt{Ls_p Ws_p f}} df \tag{6}$$

$$\sigma_{1/f4} = \frac{1}{\eta_{pin}} \int_{1}^{10^6} \frac{K_{flicker} I_c}{\sqrt{Ls_c Ws_c f}} df \tag{7}$$

$$\sigma_{1/f} = \sqrt{\sigma_{1/f1}^2 + \sigma_{1/f2}^2 + g_c^2(\sigma_{1/f3}^2 + \sigma_{1/f4}^2)} \tag{8}$$

where $K_{flicker}$ is a constant, I_p, I_c are drain current of a pixel and a column, La_p, Wa_p are the size of the amplifying transistor of a pixel, La_c, Wa_c are the size of the amplifying transistor of a column, Ls_p, Ws_p are the size of the select transistor of a pixel, Ls_c, Ws_c are the size of the select transistor of a column, and η_{pin} is the transfer efficiency of the photodiode of a CIS pixel. The noisy Macbeth chart polluted by the Gaussian component noise is shown in Fig. 5.

2.2 Non-Gaussian Noise Modeling

2.2.1 RTS Noise Modeling in Time Domain

As the two-level RTS noise is caused by electron capture and emition by the single oxide defect in the surface of Source Follower, there are usually three parameters to estimate the properties of RTS noise in time domain, i.e., mean time of capture and emition subsection τ_c, τ_e, and the amplitude ΔI in traditional research. In this paper, we assume that correlated-double sampling (CDS) has reacted on RTS noise for noise modeling of CIS [14], [27]. The pixel output and the histogram of RTS noise after CDS are shown in Fig. 6 and Fig. 7, where S/HR and S/HS are sampling at the time of reset and signal respectively. And the pixel output, CDS_Signal after CDS is given as (9). And pixel output is defined as the photoelectron number (PEN) in this study.

According to Fig. 7, a two-level RTS noise after CDS can be modeled as a discrete random variable *RTS* as Table 2,

$$CDS\_Signal = S/HS - S/HR \tag{9}$$

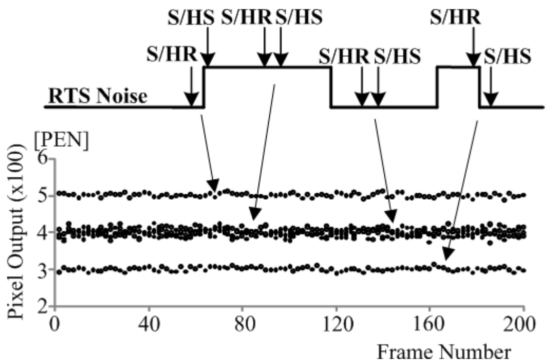

Fig. 6 RTS noise after CDS.

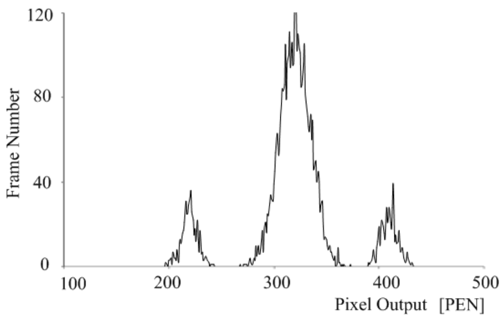

Fig. 7 Histogram of pixel output of RTS noise after CDS.

Table 2 Statistical model of RTS noise.

RTS	P_1(1-P_2)	(1-P_1)(1-P_2)+P_1P_2	P_2(1-P_1)
Value	-ΔI	0	ΔI

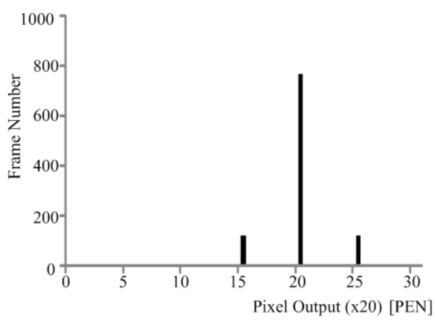

Fig. 8 Histogram of pixel output of *RTS*.

where P_1 and P_2 are the probabilities of trap occupancy of S/HR and S/HS respectively. The histogram of the ideal pixel output of *RTS* in the ideal condition is given as Fig. 8.

2.2.2 RTS Noise Modeling in Spatial Domain

As introduced before, the collective behaviors of RTS noise on a CIS are more important to achieve high quality videos and to provide a reference of video distortion to CIS manufacturing process in order to estimate the degree of distortion of motion pictures.

Firstly, the noise histogram of a CIS only with the

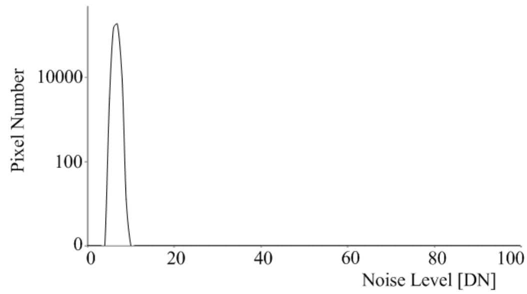

Fig. 9 Noise histogram of the Gaussian component noise, α = 5000, β = 0.0782, σ_1 = 2.0.

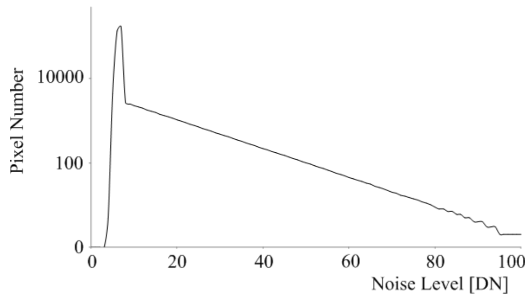

Fig. 10 Noise histogram of the Gaussian component noise and the non-Gaussian component noise, α = 5000, β = 0.0782, σ_1 = 2.0.

Gaussian component noise is calculated based on the work in [13] and shown in Fig. 9, in which the number of pixels where $NL = x$, P_{Norm} is given as (10),

$$P_{Norm}(x) = \kappa \times \frac{1}{\sqrt{2\pi}\sigma} e^{\frac{(x-\mu)^2}{2\sigma^2}} \tag{10}$$

where κ is a coefficient related to the scale parameter of the spatial distribution of the Gaussian component noise. And the vertical-axis and horizontal-axis represent the number of pixels and Digital Number (DN) of *NL* respectively.

Secondly, the noise histogram of a CIS with not only the Gaussian component noise but also the non-Gaussian component noise is calculated based on the work in [4], [11], [14], [28]–[31] and determined by the exponential distribution with two parameter α and β, which is shown in Fig. 10. However, it is not nearly enough to determine a RTS noise on a pixel merely using quantity *NL* without giving P_1, P_2 and ΔI. In our newly proposed noise modeling of CIS, all the pixels where $NL = x$ are thought to have the same values of amplitude ΔI and probabilities P_1 and P_2 for explanation at the first step as shown in Fig. 7. The number of pixels with $NL = x$, P_{RTS} is given as (11),

$$P_{RTS}(x) = \alpha \times e^{-\beta x} \tag{11}$$

where α and β are coefficients related to the scale parameter and the slope parameter of the spatial distribution of the RTS noise respectively. To build up the noise histogram in Fig. 10, we have applied numerical analysis methods to compute κ_1 and connection point Ψ in (12)–(14).

$$P_{Norm1}(x) = \kappa_1 \times \frac{1}{\sqrt{2\pi}\sigma} e^{\frac{(x-\mu)^2}{2\sigma^2}} \tag{12}$$

$$\sum_{x=0}^{N} P_{Norm}(x) = \sum_{x=0}^{\Psi_x} P_{Norm1}(x) + \sum_{x=\Psi_x+1}^{N} P_{RTS}(x) \tag{13}$$

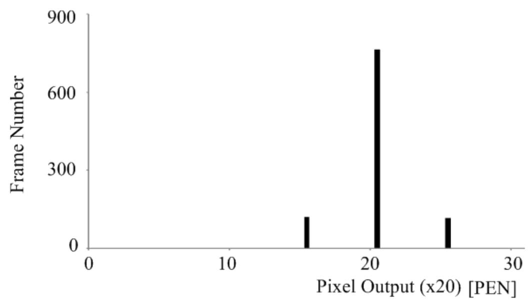

(a) RTS1, $\triangle I = 5$, $P_1 = P_2 = 0.12$

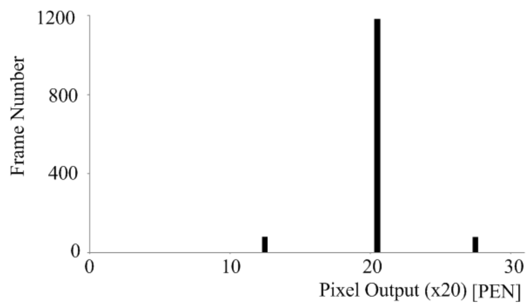

(b) RTS2, $\triangle I = 8$, $P_1 = P_2 = 0.06$

Fig. 11 Histogram of pixel output of two RTSs, RTS1 has larger ΔI than RTS2, while has smaller P_1 and P_2.

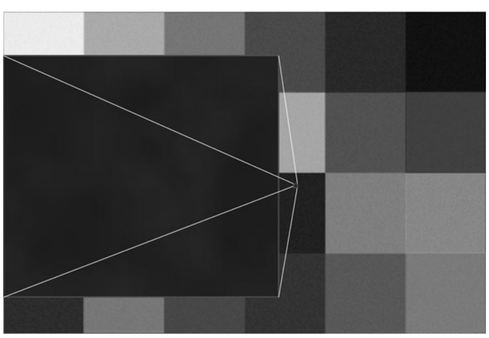

(a) Gaussian component noise only

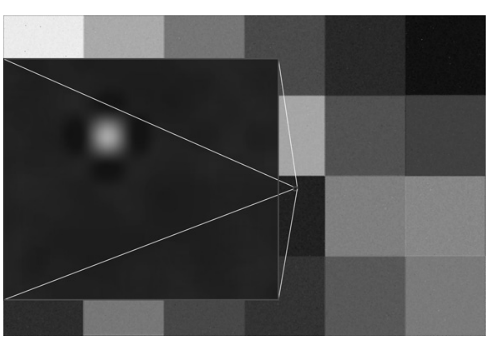

(b) Gaussian and non-Gaussian component noise

Fig. 12 Noisy Macbeth chart in two different noise conditions, $\alpha = 5000, \beta = 0.0782, \sigma_1 = 2.0$, (a) Gaussian component noise only, (b) Gaussian component noise and the non-Gaussian component noise.

$$P_{Norm1}(\Psi_x) = P_{RTS}(\Psi_x) \tag{14}$$

where κ_1 is scale parameter, Ψ_x is x-coordinate of the connection point Ψ in Fig. 10, and N is the maximum value of NL.

In fact, a CIS pixel with RTS noise usually has larger amplitude ΔI but smaller probabilities P_1 and P_2 as shown in Fig. 11, vice versa. The actual reason is that the amplitudes of the pixels on a CIS at certain NL follow a Gaussian distribution with mean μ_1 and standard deviation σ_1 instead of the same values, which is named as Gaussian amplitude in this study.

The noisy Macbeth chart with the newly proposed noise modeling of CIS is shown in Fig. 12. Figure 12 (a) only includes the Gaussian component noise. In Fig. 12 (b) both the Gaussian component noise and the non-Gaussian component noise are included.

3. Evaluation Method

In order to provide a reference to CIS manufacturing process to evaluate the quality of videos degraded by RTS noise is another objective of this paper. In previous work, PSNR is one of the most widely used methods to evaluate image quality and video quality using mean square error (MSE). However, it is not reasonable for RTS noise case since the number of pixels which are RTS noise sources is very small compared with the total pixel number of a CIS. The results of this is that motion pictures with quite different noise levels have almost identical PSNR values. RTS_VQ is a metric to evaluate the perceptual impact of distortion introduced by RTS noise and is developed to reflect the relationship between the video quality and the spatial distributions of RTS noise source.

RTS_VQ model has its inherent advantages for RTS noise compared with other video quality evaluation methods. Since on one hand, RTS_VQ emphasizes the effect of larger NL rather than equally treats all NLs; on the other hand, RTS makes use of the characteristics of the spatial distribution of RTS noise on a CIS, which are noise histograms of R, G, and B channels respectively. All these noise histograms have been calculated during the noise modeling in Sect. 2. It is therefore that only simple algebraic operations

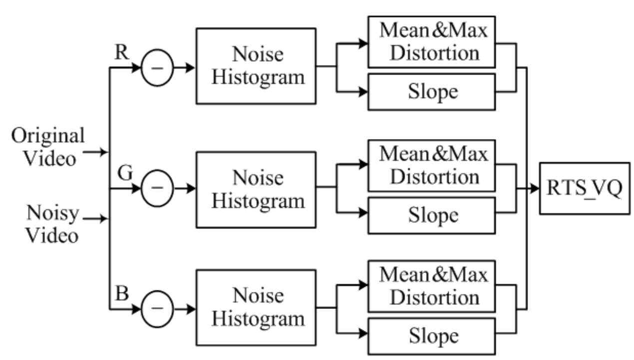

Fig. 13 Flowchart of RTS_VQ calculation.

are needed to calculate RTS_VQ by (15)–(18),

$$D_m = \sqrt{RD_m^2 + GD_m^2 + BD_m^2} \tag{15}$$

$$D_{Mi}^* = (D_{Mi} \times S\_i)^2, i = R, G, B \tag{16}$$

$$D_M = 10 \times \sqrt{D_{MR}^* + D_{MG}^* + D_{MB}^*} \tag{17}$$

$$RTS\_VQ = D_m + 0.005 \times D_M \tag{18}$$

where D_m is the mean distortion of the video; RD_m, GD_m, and BD_m are mean distortion of R, G and B channels respectively; D_M is the maximum distortion of the video; D_{MR}, S_R, D_{MG}, S_G, D_{MB}, and S_B are maximum distortion and slope of R, G and B channels respectively, and D_{Mi}^* is just a temporary variable for calculation; 0.005 is the maximum distortion weight parameter which is chosen based on several primitive psychophysics experiments [22]; 10 is the scale parameter in order to provide a reasonable value of RTS_VQ. If the value of maximum distortion weight parameter is smaller than 0.005, the contribution of pixels on the large noise level will be decreased. Consequently, the RTS_VQ becomes a averaging value like PSNR. In contrast, if the value of maximum distortion weight parameter is larger than 0.005, the contribution of pixels on the large noise level will be increased. And the mean distortion, which indicates the major information of an image, will be immensely weakened. And the flowchart of RTS_VQ calculation is shown in Fig. 13.

4. Experimental Results and Discussion

We developed a video camera exposure simulator (VCES) to simulate the imaging process of a CIS, the flowchart of which is shown in Fig. 3. The noise free frame of VCES is a Macbeth chart shown in Fig. 2. The proposed noise modeling of CIS is included in VCES. The VCES in experiments is analogous to a video camera, and parameters configuration of them are similar and given in Table 3. The output of VCES is a motion picture with 30 frames per second, in which a frame is a 480×720 Macbeth chart. And one of the experimental results of Macbeth chart with the proposed RTS noise model is shown in Fig. 14.

As shown in Table 3, the size of a CIS pixel in VCES is a $2\,\mu\text{m} \times 2\,\mu\text{m}$ submicron MOSFET device pronounced by RTS noise. In order to test the proposed noise modeling of CIS, five different noisy conditions are listed in Table 4, where CP denotes the connected point in the noise histogram. In RTS_0, only the Gaussian noise is considered. In RTS_{1-4}, RTS noise is also included. The noise histograms of RTS_{1-4} are shown in Fig. 15 and that of RTS_0 has been shown in Fig. 10, in which all the noise histograms are in the condition of Gaussian amplitude where $\sigma_1 = 2$, the default value in VCES. According to the experimental results in RTS_1, the pixel output of $P_{686,360}$ and $P_{89,40}$ are shown in Fig. 16 (a) and (b) respectively.

Video quality evaluation metrics PSNR, DVQ, MQE, and VQM have been used for comparison to demonstrate the effectiveness of RTS_VQ. As a result of that VQM is proposed to improve the performance of DVQ [20], only the values of PSNR, MQE, and VQM for RTS_{0-4} are calculated. The definition of PSNR is given as (19)–(23),

$$MSE_R = \frac{1}{LMN} \sum_{i=0}^{L} \sum_{j=0}^{M} \sum_{k=0}^{N} (O_{i,j,k_R} - I_{i,j,k_R})^2 \tag{19}$$

$$MSE_G = \frac{1}{LMN} \sum_{i=0}^{L} \sum_{j=0}^{M} \sum_{k=0}^{N} (O_{i,j,k_G} - I_{i,j,k_G})^2 \tag{20}$$

$$MSE_B = \frac{1}{LMN} \sum_{i=0}^{L} \sum_{j=0}^{M} \sum_{k=0}^{N} (O_{i,j,k_B} - I_{i,j,k_B})^2 \tag{21}$$

$$MSE_V = \frac{1}{3} \times (MSE_R + MSE_G + MSE_B) \tag{22}$$

Table 3 Configuration of VCES.

Parameter	Value	Parameter	Value
Focus	4	**Intensity**	320
ISO	200	**Shutter Speed**	0.004s
Pixel Pitch	2 μm	**Color Temp**	5500K
Sensor Temperature	300K		

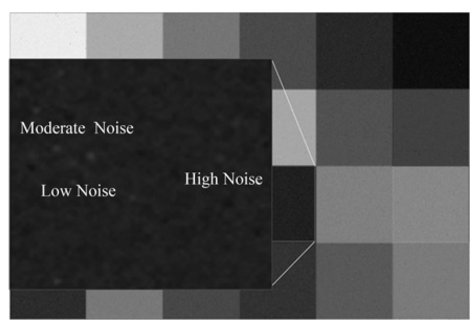

Fig. 14 Simulation results of Macbeth chart with the proposed noise modeling of CIS.

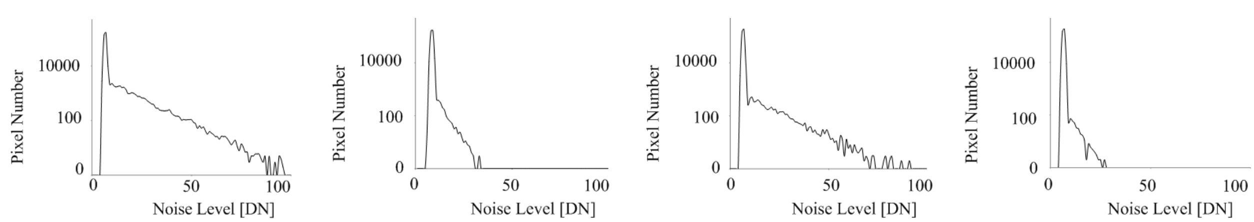

(a) RTS_1 (b) RTS_2 (c) RTS_3 (d) RTS_4

Fig. 15 Noise histogram of RTS_{1-4} from (a) to (d).

$$PSNR = 10\lg\left(\frac{Peak\_Signal^2}{MSE_V}\right) \tag{23}$$

where O_{i,j,k_R}, O_{i,j,k_G}, O_{i,j,k_B} are gray scale of red, green, and blue channels of a noisy motion picture; I_{i,j,k_R}, I_{i,j,k_G}, I_{i,j,k_B} are gray scale of red, green, and blue channels of the reference motion picture; L is frame number; M and N are the width and height of the CIS in VCES; MSE_R, MSE_G, and MSE_B are MSE values of red, green, and blue channels of a noisy motion picture; MSE_V is MSE value of a noisy motion picture; and Peak_Signal is the maximum gray scale of the frames in VCES.

As the results of PSNR and RTS_VQ for RTS_{0-4} shown in Table 4, PSNR remains identical as expected, while RTS_VQ can evaluate the video distortion by RTS noise well. It is also shown in Table 4 is that RTS_VQ decreases indicating worse video quality as σ_1 decreases resulting from RTS noise with large amplitude appears. And the noise histogram of $\sigma_1 = 0.5$ is more fitting to the physical experimental results. According to the results in Table 4 and Table 5, PSNR and VQM are almost identical for RTS noise case. MQE seems to be resolvable compared to PSNR and VQM. However, there is no rule for the values of MQE to follow in the changing of RTS noisy situations. More experimental results for comparison between RTS_VQ and PSNR as the change of α and β are shown in Fig. 17. Based on the experimental results in Table 4 and Fig. 17, the effectiveness of the proposed video quality evaluation method RTS_VQ is demonstrated.

As shown in Fig. 14, different noise levels, high noise, moderate noise and low noise are marked with white circles with the newly proposed noise modeling of CIS. Especially, we have a small area of the noisy Macbeth charts enlarged to emphasize the impact of noise on a frame. Figure 12 (a) shows some irregular streaks caused by the Gaussian component noise, and in Fig. 12 (b) and Fig. 14, prominent spots caused by RTS noise appear. Further, it can be seen from the result of motion pictures that flickers caused by RTS noise significantly affect human visual sensitivity which could be reflected by the noise histogram changing in Fig. 15. As shown in Fig. 15 (a) and (c), the RTS_1 and the RTS_3 have the same values of parameter β but the different values of α. Correspondingly, the straight downward-sloping lines of the noise histograms in Fig. 15 (a) and (c) have same shape but different scales. So are the RTS_2 and the RTS_4 in Fig. 15 (b) and (d). Comparatively, the RTS_1 and the RTS_2 shown in Fig. 15 (a) and (b) respectively have the same values of parameter α but the different values of β, which results in totally different shape of noise histograms. And the RTS_2 and the RTS_4 in Fig. 15 (b) and (d) are in the same way. In addition, as the pixel outputs shown in Fig. 16 (a) and (b),

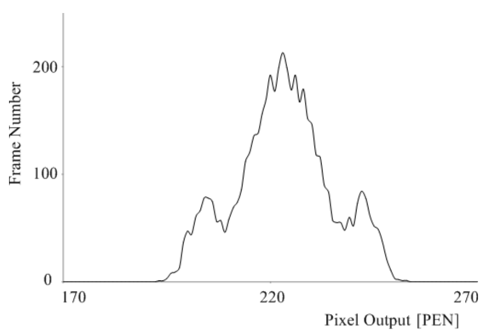

(a) Pixel output of $P_{686,360}$

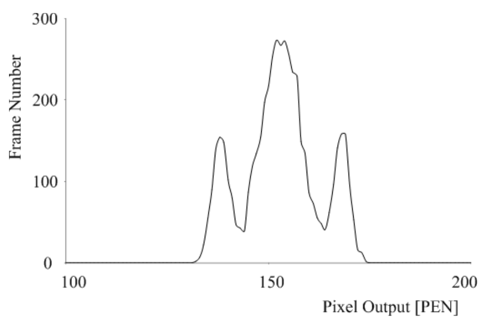

(b) Pixel output of $P_{89,40}$

Fig. 16 Experimental results of pixel output of (a) $P_{686,360}$ and (b) $P_{89,40}$.

Table 4 PSNR and RTS_VQ values for RTS_{0-4}.

Noise Cond	RTS		CP		Fixed Amplitude		Gaussian Distributed Amplitude			
							σ_1 = 2		σ_1 = 0.5	
	α	β	Ψ_x	Ψ_y	*PSNR*	*RTS_VQ*	*PSNR*	*RTS_VQ*	*PSNR*	*RTS_VQ*
RTS_0	-	-	-	-	14.38	13.25	14.38	13.25	14.38	13.25
RTS_1	5000	0.0782	9	2474	14.38	23.03	14.38	22.91	14.38	21.97
RTS_2	5000	0.2482	10	418	14.38	15.81	14.38	15.64	14.38	15.53
RTS_3	1000	0.0782	10	457	14.38	21.44	14.38	21.24	14.38	21.08
RTS_4	1000	0.2482	10	84	14.38	14.99	14.38	14.73	14.38	14.64

Table 5 MQE and VQM values for RTS_{0-4}.

Noise Cond	RTS		CP		Fixed Amplitude		Gaussian Distributed Amplitude			
							σ_1 = 2		σ_1 = 0.5	
	α	β	Ψ_x	Ψ_y	*MQE*	*VQM*	*MQE*	*VQM*	*MQE*	*VQM*
RTS_0	-	-	-	-	6.07	0.76	6.07	0.76	6.07	0.76
RTS_1	5000	0.0782	9	2474	6.35	0.77	5.82	0.77	5.69	0.77
RTS_2	5000	0.2482	10	418	6.00	0.76	5.99	0.76	5.96	0.76
RTS_3	1000	0.0782	10	457	5.59	0.76	5.91	0.76	5.88	0.76
RTS_4	1000	0.2482	10	84	5.77	0.76	5.94	0.76	5.73	0.76

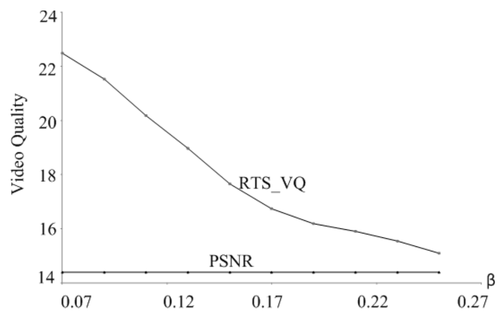

(a) α = 5000

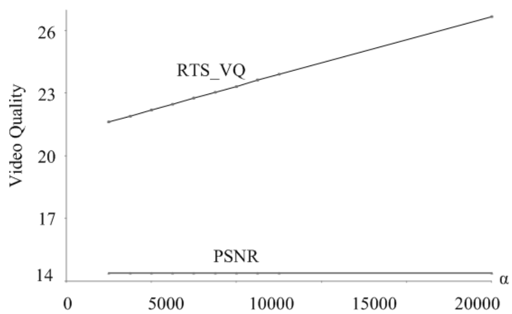

(b) β = 0.07

Fig. 17 Experimental results with parameters α and β changing of (a) and (b) respectively.

$P_{686,360}$ has larger amplitude ΔI but smaller probabilities P_1 and P_2 compared with $P_{89,40}$. The difference of pixel output between Fig. 15 and Fig. 11 is that the the histogram in Fig. 16 is with Gaussian shape because of the Gaussian component noise in the proposed noise modeling of CIS.

5. Conclusions

An RTS noise modeling based on numerical and statistical approach and a quantative evaluation method in motion pictures were developed in this study. According to the experimental results of the proposed RTS noise modeling, the values of α, β and σ_1 have a significant impact on the noise histogram and video quality of a CIS. The effectiveness of RTS_VQ is also demonstrated compared with PSNR, so that it is possible to provide a reference to CIS manufacturing process to evaluate the quality of motion pictures distorted by RTS noise.

The conclusion is that RTS noise becomes severer and the flickers caused by RTS noise more significantly affect the human visible sensations as the value of parameter α decreases, parameter β increases or parameter σ_1 decreases. Then a high quality motion picture with quantificational analysis of noise modeling of CIS is obtained based on those works mentioned above.

At last, because there is only a marginal difference of the values of RTS_VQ and PSNR between RTS_0, RTS_2 and RTS_4, it means the degree of video distortion is acceptable and reasonable for CIS manufacturing process to control the cost of RTS noise source cancelation since it does not have to motivate a noise histogram like RTS_0.

Based on the simulation results, the satisfactory performance of the proposed RTS noise modeling and video quality evaluation method encourages us to utilize this method in different applications.

Acknowledgements

We deeply appreciate for the contributions of Dr. Hirofumi Sumi, Mr. Hiroaki Ammo and Mr. Kazuyuki Matsushima from Sony Corporation in Tokyo Japan.

References

[1] B.S. Carlson, "Comparison of modern CCD and CMOS image sensor technologies and systems for low resolution imaging," Sensors, Proc. IEEE, vol.1, no.1, pp.171–176, 2002.
[2] Dalsa Corp., "Electronic shuttering for high speed CMOS machine vision applications," Photonik, pp.2–4, May 2005.
[3] A. Konczakowska, J. Cichosz, and A. Szewczyk, "A new method for RTS noise of semiconductor devices identification," IEEE Trans. Instrum. Meas., vol.57, no.6, pp.1199–1206, June 2008.
[4] C. Leyris, S. Pilorget, M. Marin, M. Minondo, and H. Jaouen, "Random telegraph signal noise SPICE modeling for circuit simulators," Solid State Device Research Conference, pp.187–190, Sept. 2007.
[5] T. Goudon, V. Miljanovic, and C. Schmeiser, "On the Shockley-read-hall model: Generation-recombination in semiconductors," www.hyke.org/preprint/2006/01, 2006.
[6] G. Ghibaudo and T. Boutchacha, "Electrical noise and RTS fluctuations in advanced CMOS devices," Microelectronics Reliability, vol.42, pp.573–582, 2002.
[7] T. Nuns, G. Quadri, J.P. David, and O. Gilard, "Annealing of proton-induced random telegraph signal in CCDs," IEEE Trans. Nucl. Sci., vol.54, no.4, pp.1120–1128, Aug. 2007.
[8] E. Hoekstra, "Large signal excitation measurement techniques for RTS noise in MOSFETs," Int. Conf. on Computer as a Tool, vol.2, pp.1863–1866, Nov. 2005.
[9] A.P. van der Wel, E.A.M. Klumperink, L.K.J. Vandamme, and B. Nauta, "Modeling random telegraph noise under switched bias conditions using cyclostaionary RTS noise," IEEE Trans. Electron Devices, vol.50, no.5, pp.1370–1377, May 2003.
[10] C. Leyris, F. Roy, and M. Marin, "Modeling of the temporal pixel to pixel noise of CMOS image sensors," Int. Image Sensor Workshop, 2007.
[11] C. Leyris, J.C. Vildeuil, F. Roy, F. Martinez, M. Valenza, and A. Hoffmann, "Response of correlated double sampling CMOS imager circuit to random telegraph signal noise," Int. Caribbean Conf. on Devices, Circuits and Systems, pp.109–114, 2006.
[12] A. Konczakowska, J. Cichosz, and A. Szewczyk, "A new method for identification of RTS noise," Bulletin of the Polish Academy of Science, Technical Science, vol.54, no.4, pp.457–460, 2006.
[13] S. Kobayashi, M. Saitoh, and K. Uchida, "Id fluctuations by stochastic single-hole trappings in high-k dielectric p-MOSFETs," Symposium on VLSI Technology, pp.78–79, 2008.
[14] X.Y. Wang, P.R. Rao, A. Mierop, and A.J.P. Theuwissen, "Random telegraph signal in CMOS image sensor pixels," Int. Electron Devices Meeting (IEDM06), pp.115–118, Dec. 2006.
[15] B. Picinbono, "Moments and polyspectra of the discrete-time random telegraph signal," IEEE Trans. Inf. Theory, vol.46, no.7, pp.2735–2739, Nov. 2000.
[16] C.J.B. Lambrecht and M. Kunt, "Characterization of human visual sensitivity for video imaging applications," Signal Process., vol.67, no.3, pp.255–269, 1998.
[17] J. Lubin, "A human vision system model for objective picture quality measurements," Int. Broadcasting Convention, pp.498–503, Sept. 1997.

[18] X.K. Yang, W.S. Ling, Z.K. Lu, E.P. Ong, and S.S. Yao, "Just noticeable distortion model and its applications in video coding," Signal Process., Image Commun., vol.20, no.7, pp.662–680, 2005.
[19] A.H. Fujii, "Evaluation method for objective movie quality," IEEE Pacific Rim Conf. on Communications, Computers and Signal Processing, vol.2, pp.725–728, Aug. 1997.
[20] F. Xiao, "DCT-based video quality evaluation," MSU Graphics and Media Lab (Video Group), 2000.
[21] A.B. Watson, J. Hu, and J.F. McGowan III, "Digital video quality metric based on human vision," J. Electronic Imaging, vol.10, no.1, pp.20–29, 2001.
[22] W. Ji, H. Shi, and Y. Wang, "Objective evaluation for compressed video quality based on fuzzy synthetic judgment," Lect. Notes Comput. Sci. (FSKD06), vol.4223, pp.753–761, Sept. 2006.
[23] D. Pascale, "RGB coordinates of the Macbeth colorchecker," Technical Report, BabelColor, pp.1–16, 2003.
[24] J.Y. Huo, Y.L. Chang, J. Wang, and X.X. Wei, "Robust automatic white balance algorithm using gray color points in images," IEEE Trans. Consum. Electron., vol.52, no.2, pp.541–546, May 2006.
[25] Y. Kim, H.S. Lee, A.W. Morales, and S.J. Ko, "A video camera system with enhanced zoom tracking and auto white balance," IEEE Trans. Consum. Electron., vol.48, no.3, pp.428–434, Aug. 2002.
[26] Y.C. Liu, W.H. Chan, and Y.Q. Chen, "Automatic white balance for digital still camera," IEEE Trans. Consum. Electron., vol.41, no.3, pp.460–466, Aug. 1995.
[27] C. Xu, S. Chao, and M. Chan, "A new correlated double sampling (CDS) technique for low voltage design environment in advanced CMOS technology," Proc. Solid-State Circuits Conference (ESSCIRC02), pp.117–120, Sept. 2002.
[28] K. Abe, S. Sugawa, S. Watabe, N. Miyamoto, A. Teramoto, Y. Kamata, K. Shibusawa, M. Toita, and T. Ohmi, "Random telegraph signal statistical analysis using a very large-scaleArray TEG with 1M MOSFETs," IEEE Symp. on VLSI Technology, pp.210–211, June 2007.
[29] K. Abe, T. Fujisawa, A. Teramoto, S. Watabe, S. Sugawa, and T. Ohmi, "Anomalous RTS extractions from a very large number of n-MOSFETs using TEG with 0.47 Hz - 3.0 MHz sampling frequency," Int. Conf. on Solid State Devices and Materials, pp.888–889, 2008.
[30] S.T. Sugawa, "Random telegraph signal noises in small MOS devices," IEICE Technical Report, ICD2008-75, Oct. 2008.
[31] S.T. Sugawa, K. Abe, T.F. Fujisawa, S. Watabe, R. Kuroda, and N. Miyamoto, "Statistical analysis of random telegraph signals in the transistors equivalent to pixel source followers using a large-scale array TEG," ITE Technical Report, vol.I.32, no.19, pp.9–12, 2008.

Deng Zhang is currently pursuing his master degree at Waseda University Graduate school of Information, Production, and Systems in Japan since 2007. He received his B.S. degree in Software Engineering from Nanjing University, China, 2007. His main research interests are the CMOS image sensor, medical image processing, and robot vision. E-mail: zhdnstar@fuji.waseda.jp

Jegoon Ryu is currently pursuing his PhD at Waseda University Graduate school of Information, Production, and Systems in Japan since 2006. He received his B.S. and the M.S. degrees in Electronic Engineering from Inha University, Incheon, Korea, in 1999 and in 2004, respectively. From 1999 to 2001, he was a junior researcher at R&D of MECA Information communication Co. Ltd. From 2004 to 2006, he was a lecturer at Korea Polytechnic University and a researcher at Intelligence Healthcare system Research Center. His main research interests are the CMOS image sensor, robot vision, and medical image processing. He is currently a student member of IEEE, IEEJ, and RSJ. E-mail: jkryu@ruri.waseda.jp

Toshihiro Nishimura is currently a professor of Information Architecture, Graduate school of Information, Production and System and Faculty of School of Creative Science and Engineering, Waseda University since 2003. He received the Dr. Eng. Degree from the University of Tokyo in 1991. His research interests are the artificial human retinal prosthesis, CMOS image sensor, robot vision, medical ultrasonic imaging, neural network, self organized map, nerve physiology, cardiovascular system, and all the power electronics on human affairs and space missions. He is previous Chairman of Committee on Medical and Biological Engineering IEE Japan, Trustee of Medical Ultrasonics Society, Councilor of IEEE power Electronics Society and a Member of JSMBE, IEEJ and IEEE, the general chair of IEEE/ISICE 2007, 2008. He has decorated many from the society of IEEJ-C, IEEE and also European societies. E-mail: tosi-hiro@waseda.jp